Journal of Inorganic Biochemistry 113 (2012) 47–54

Contents lists available at SciVerse ScienceDirect

Journal of Inorganic Biochemistry

journal homepage: www.elsevier.com/locate/jinorgbio

Osmium(IV) complexes with 1*H*- and 2*H*-indazoles: Tautomer identity versus spectroscopic properties and antiproliferative activity

Gabriel E. Büchel [a], Iryna N. Stepanenko [a], Michaela Hejl [a], Michael A. Jakupec [a,c], Bernhard K. Keppler [a,c], Petra Heffeter [b,c], Walter Berger [b,c], Vladimir B. Arion [a,*]

[a] University of Vienna, Institute of Inorganic Chemistry, Währinger Strasse 42, A-1090 Vienna, Austria
[b] Department of Medicine I, Institute of Cancer Research, Medical University of Vienna, Borschkegasse 8a, A-1090 Vienna, Austria
[c] Research Platform "Translational Cancer Research", University of Vienna and Medical University of Vienna, Vienna, Austria

ARTICLE INFO

Article history:
Received 2 February 2012
Received in revised form 2 April 2012
Accepted 2 April 2012
Available online 10 April 2012

Keywords:
Osmium(IV) complexes
1*H*- and 2*H*-indazole tautomers
Antiproliferative activity

ABSTRACT

A one-pot synthesis of osmium(IV) complexes with two different tautomers of indazole, 1*H*-indazole and 2*H*-indazole, namely $(H_2ind)[Os^{IV}Cl_5(2H\text{-ind})]$ (**1**) and $(H_2ind)[Os^{IV}Cl_5(1H\text{-ind})]$ (**2**) is reported. Both compounds have been comprehensively characterized by NMR spectroscopy, ESI (electrospray ionization) mass spectrometry, electronic absorption spectroscopy, IR spectroscopy, cyclic voltammetry and tested for antiproliferative activity *in vitro* in three human cancer cell lines, CH1 (ovarian carcinoma), A549 (non-small cell lung cancer) and SW480 (colon carcinoma), as well as *in vivo* in a Hep3B SCID mouse xeno-transplantation model. 2*H*-Indazole tautomer stabilization in **1** has been confirmed by X-ray diffraction.

1. Introduction

Indazoles are rare in nature, and so far only three natural products based on an indazole ring have been isolated [1]. These are the indazole alkaloids nigellicine [2], nigeglanine [3], and nigellidine [4]. The total syntheses of nigellicine and nigeglanine are also well documented [5,6]. The indazole ring system is of much current interest as partial structure of a large number of biologically active compounds. Different aspects of pharmaceutical and other useful applications of indazoles have been reviewed [7,8]. Some substituted indazoles exhibit relevant biological properties for development as anticancer drugs [9–15]. One of the tetrasubstituted indazoles, namely, CI-958, entered clinical trials for prostate cancer treatment about a decade ago [16]. From the unsubstituted indazole derivatives the most prominent example is the ruthenium(III) compound $(H_2ind)[trans\text{-}Ru^{III}Cl_4(Hind)_2]$ (KP1019, Hind = 1*H*-indazole), which is now in clinical trials as an anticancer agent against metastatic solid tumors [17,18]. Of potential interest are also complexes closely related to $(H_2im)[trans\text{-}Ru^{III}Cl_4(DMSO)(Him)]$ (NAMI-A, Him = imidazole) [19], an investigational drug which is currently evaluated in a clinical phase II trial for its capacity of inhibiting the process of metastasis, namely $(H_2ind)[trans\text{-}Ru^{III}Cl_4(DMSO)(Hind)]$ [20] and its osmium counterpart [21].

The indazole heterocycle is normally referred to as 1*H*-indazole, although it has two other potential tautomers 2*H*-indazole and 3*H*-indazole (Chart 1).

The 1*H*-indazole was found to be the dominant tautomer in the gaseous state and in aqueous solution, and this result is not reversed in the excited state by a solvent effect [1,7]. X-ray diffraction studies of *N*-unsubstituted indazoles confirm the general preference for 1*H*-tautomers in the solid state [22–30]. 1*H*-Indazoles have benzenoid properties (are aromatic in nature), while 2-substituted 2*H*-indazoles have ortho-quinoid character [31,32]. 3*H*-Indazoles lack heteroaromatic character and are very rare [33].

There is some evidence regarding the influence of the tautomeric equilibrium in indazoles on the different biological properties [34–38]. However, the effect of tautomer identity on the antiproliferative activity, biological mechanisms involved, and other physico-chemical properties, which can have an impact on pharmacokinetic and

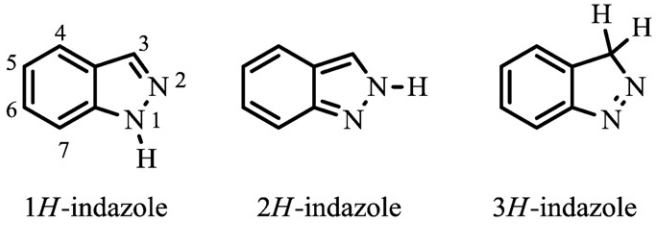

1*H*-indazole 2*H*-indazole 3*H*-indazole

Chart 1. The tautomers of indazole.

* Corresponding author.
E-mail address: vladimir.arion@univie.ac.at (V.B. Arion).

0162-0134
doi:10.1016/j.jinorgbio.2012.04.001

pharmacodynamic behaviors in the case of metal complexes with indazole remains unexplored.

Herein we report on the one-pot synthesis of two complexes, (H_2ind)[$Os^{IV}Cl_5$(2*H*-ind)] (**1**) and (H_2ind)[$Os^{IV}Cl_5$(1*H*-ind)] [39] (**2**). Stabilization of the 2*H*-form of indazole and binding to osmium(IV) via nitrogen atom N1 was found in **1**. This is only the second example of indazole coordination via N1 to a transition metal ion [40]. In addition, we studied the stability of both isomers in aqueous solution and compared their antiproliferative activity *in vitro* in three human cancer cell lines CH1 (ovarian carcinoma), SW480 (colon carcinoma) and A549 (non-small cell lung cancer) and *in vivo* in a Hep3B SCID mouse xeno-transplantation model in order to establish whether tautomer identity in **1** and **2** has any effect on biological properties. The antiproliferative activity of (H_2ind)[$Os^{IV}Cl_5$(2*H*-ind)] (**1**) was found to be superior to that of (H_2ind)[$Os^{IV}Cl_5$(1-*H*-ind)] (**2**) in one of three human cancer cell lines applied but inferior in the *in vivo* xeno-transplantation model.

2. Experimental section

2.1. Materials

The starting compounds [$(DMSO)_2H]_2[OsCl_6]$ [41,42] and $(H_2ind)_2[OsCl_6]$ [43] were synthesized as previously reported in the literature. OsO_4 (99.8%) and $N_2H_4{\cdot}2HCl$ were purchased from Johnson Matthey and Fluka, correspondingly, while 1*H*-indazole was from Aldrich. All these chemicals were used without further purification. (H_2ind)[$OsCl_5$(2*H*-Hind)] (**1**) and (H_2ind)[$OsCl_5$(1*H*-Hind)] (**2**) were prepared under argon atmosphere using standard Schlenk techniques (Chart 2).

2.2. Synthesis of (H_2ind)[$OsCl_5$(κN1-2H-ind)] (**1**) and (H_2ind)[$OsCl_5$(κN2-1H-ind)] (**2**)

A suspension of $(H_2ind)_2[OsCl_6]$ (100 mg, 0.16 mmol) in ethanol (2 ml) was heated in a Schlenk tube at 100 °C (oil bath) for 2 h. After cooling to room temperature the violet precipitate of **1** was filtered off, recrystallized from water/acetone (1:1), and dried in vacuo. Yield of **1**: 27 mg, 27%. By reducing the volume of the filtrate to one half a brown solid of **2** was formed. This was filtered off, washed with cold ethanol (2 ml) and dried in vacuo. Yield of **2**: 22 mg, 22%. Analytical data for **1**: Anal. Calcd for $C_{14}H_{13}Cl_5N_4Os{\cdot}H_2O$ (**1**·H_2O) (M_r = 622.79 g/mol): C, 27.00; H, 2.43; N, 9.00. Found: C, 27.41; H, 2.56; N, 8.85. ESI-MS in MeOH (negative): *m/z* 485 $[Os^{IV}Cl_5(Hind)]^-$, 367 $[Os^{IV}Cl_5]^-$, 333 $[OsCl_4]^-$. MIR, cm^{-1}: 603, 626, 664, 736, 784, 846, 872, 928, 978, 1077, 1136, 1181, 1238, 1309, 1382, 1441, 1505, 1584, 1618, 2348, 2933, 2975, 3135, 3487 and 3547. FIR, cm^{-1}: 159, 171, 203, 223, 283, 293, 308, 319, 350, 398, 427, 443, 537, 561 and 614. UV–vis (H_2O), λ_{max}, nm (ε, $M^{-1}\,cm^{-1}$): 288 (10 095), 362 (8 912), 406 sh (3 236), 560 (5 075), 598 (4 443). UV–vis (THF), λ_{max}, nm (ε, $M^{-1}\,cm^{-1}$): 367 (9 147), 408 sh (3 996), 518 (3 853), 593 (326). UV–vis (DMF), λ_{max}, nm (ε, $M^{-1}\,cm^{-1}$): 368 (10 000), 408 sh (3 949), 510 (4 080), 595 (251). UV–vis (DMSO), λ_{max}, nm (ε, $M^{-1}\,cm^{-1}$): 367 (5 687), 409 sh (2 752), 521 (2 794), 597 (304). ^1H NMR (DMSO-d_6, 500.32 MHz): δ −14.54 (s, 1H, H_3), −0.43 (t, 1H, *J* = 7.67 Hz, H_6), 2.81 (d, 1H, *J* = 8.56 Hz, H_4), 4.52 (d, 1H, *J* = 8.83 Hz, H_7), 6.66 (t, 1H, *J* = 6.91 Hz, H_5), 7.11 (t, 1H, *J* = 7.19 Hz, $H_{5'}$), 7.34 (t, 1H, *J* = 7.34 Hz, $H_{6'}$), 7.54 (d, 1H, *J* = 8.42 Hz, $H_{7'}$), 7.76 (d, 1H, *J* = 8.12 Hz, $H_{4'}$), 8.07 (s, 1H, $H_{3'}$), 14.25 (s, 1H, H_2) ppm. $^{13}C\{^1H\}$ NMR (DMSO-d_6, 125.82 MHz): δ 58.55 (C_9), 99.06 (C_7), 104.60 (C_5), 110.56 ($C_{7'}$), 120.67 ($C_{5'}$), 120.98 ($C_{4'}$), 123.22 ($C_{9'}$), 126.41 ($C_{6'}$), 133.82 ($C_{3'}$), 140.32 ($C_{8'}$), 157.09 (C_4), 177.15 (C_6), 184.29 (C_8), 299.7 (C_3) ppm. ^{15}N NMR (DMSO-d_6, 50.70 MHz): δ 85.9 (N_2) ppm. Suitable crystals of **1**·H_2O for X-ray diffraction study were grown from a solution of **1** in DMSO.

Analytical data for **2**: ESI-MS in MeOH (negative): *m/z* 485 $[Os^{IV}Cl_5(Hind)]^-$, 367 $[Os^{IV}Cl_5]^-$. UV–vis (H_2O), λ_{max}, nm (ε, $M^{-1}\,cm^{-1}$): 250 (11 134), 257 (10 982), 271 (10 841), 279 (11 395), 284 (11 751) 294 sh (9 593), 358 (8 882), 401 sh (4 770), 449 sh (2 411), 556 (669), 594 (632). UV–vis (THF), λ_{max}, nm (ε, $M^{-1}\,cm^{-1}$): 253 (10 264), 287 (12 955), 294 sh (11 844), 365 (9 728), ~510 sh (356). UV–vis (DMF), λ_{max}, nm (ε, $M^{-1}\,cm^{-1}$): 287 (15 146), 294 sh (13297), 366 (12 140), ~510 sh (244). UV–vis (DMSO), λ_{max}, nm (ε, $M^{-1}\,cm^{-1}$): 285 (11 680), 295 sh (9 562), 364 (8 249), 514 (503), 596 (51). UV–vis (MeOH), λ_{max}, nm (ε, $M^{-1}\,cm^{-1}$): 249 (9 450), 284 (12 152), 293 (10 019), 361 (8 780), 524 (562). ^1H NMR (DMSO-d_6, 500.32 MHz): δ −4.54 (s, 1H, H_3), 3.06 (t, 1H, *J* = 7.7 Hz, H_6), 5.90 (d, 1H, *J* = 7.5 Hz, H_4), 7.11 (t, 1H, *J* = 7.4 Hz, $H_{5'}$), 7.34 (t, 1H, *J* = 7.6 Hz, $H_{6'}$), 7.53 (d, 1H, *J* = 8.4 Hz, $H_{7'}$), 7.76 (d, 1H, *J* = 8.1 Hz, $H_{4'}$), 8.07 (s, 1H, $H_{3'}$), 8.23 (t, 1H, *J* = 7.6 Hz, H_5), 10.85 (d, 1H, *J* = 8.5 Hz, H_7), 17.76 (s, 1H, H_1) ppm. The analytical data for **2** were identical with those reported previously for the same compound prepared via three-step synthesis [39].

2.3. Physical measurements

Elemental analyses were performed by the Microanalytical Laboratory of the Faculty of Chemistry of the University of Vienna. MIR spectra were measured by using an ATR unit with a Perkin-Elmer 370 FTIR 2000 instrument (4000–400 cm^{-1}). FIR spectra were recorded on the same instrument in transmission mode using CsI-pellets. UV–vis spectra were measured on a Perkin-Elmer Lambda 20 UV–vis spectrophotometer using samples dissolved in DMSO, DMF (dimethylformamide), THF (tetrahydrofuran), water or methanol. Electrospray ionization mass spectrometry was carried out with a Bruker Esquire 3000 instrument (Bruker Daltonics, Bremen, Germany) by using methanol and water as solvents. Expected and measured isotope distributions were compared. The X-band EPR spectra were recorded on a modified Varian E-4 spectrometer (Chicago, Roosevelt University). Cyclic voltammograms were measured in a three-electrode cell using a 2 mm diameter glassy carbon disk working electrode, a

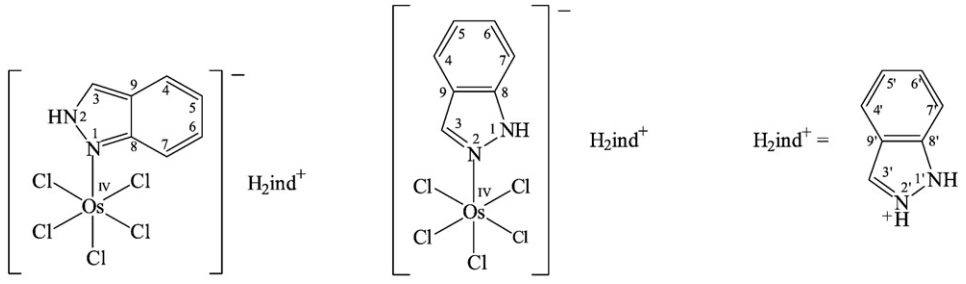

(H_2ind)[$Os^{IV}Cl_5$(*kN1*-2*H*-ind)] (**1**) (H_2ind)[$Os^{IV}Cl_5$(*kN2*-1*H*-ind)] (**2**)

[a]Atom labeling was introduced for assignments of resonances in NMR spectra.

Chart 2. Compounds reported in this work.[a].

platinum auxiliary electrode and an $Ag|Ag^+$ reference electrode containing 0.1 M $AgNO_3$. Measurements were performed at room temperature using an EG&G PARC potentiostat/galvanostat model 273A. Deareation of solutions was accomplished by passing a stream of argon through the solution for 5 min prior to the measurement and then maintaining a blanket atmosphere of argon over the solution during the measurement. The potentials were measured in 0.2 M (n-Bu_4N)[BF_4]/DMSO using [Fe(η^5-C_5H_5)$_2$] ($E^{ox}_{1/2} = +0.68$ V vs NHE (normal hydrogen electrode)) [44] as internal standard and are quoted relative to NHE. The ^1H, ^{13}C and ^{15}N NMR spectra were recorded at 500.32, 125.82 and 50.70 MHz on a Bruker DPX500 (Ultrashield Magnet) in DMSO-d_6. 2D ^{13}C,^1H HSQC,^{15}N,^1H HSQC (heteronuclear single quantum coherence), ^{13}C,^1H HMBC (heteronuclear multi-bond correlation spectroscopy) and ^1H,^1H COSY (correlation spectroscopy) experiments were also performed.

2.4. Crystallographic structure determination

X-ray diffraction measurement was carried out on a Bruker X8 APEXII CCD diffractometer. Single crystal of **1**·H_2O was positioned at 40 mm from the detector, and 972 frames were measured, each for 20 s over 1° scan width. The data was processed using SAINT software [45]. Crystal data, data collection parameters, and structure refinement details are given in Table 1. The structure was solved by direct methods and refined by full-matrix least-squares techniques. Os, Cl and O atoms were refined with anisotropic displacement parameters, while C and N atoms isotropically. H atoms were inserted in calculated positions and refined with a riding model. The coordinated 2*H*-indazole was found to be disordered over two positions related by a plane of symmetry through Os1, three chloride ligands, atoms N1 and C1. The indazolium cation was found to be disordered over four symmetry related (pairwise) positions. The following software programs and computer were used: structure solution, *SHELXS-97*; refinement, *SHELXL-97* [46]; molecular diagrams, *ORTEP-3* [47]; computer, Intel CoreDuo.

2.5. Cell lines and culture conditions

CH1 (ovarian carcinoma, human) cells were donated by Lloyd R. Kelland (CRC Centre for Cancer Therapeutics, Institute of Cancer Research, Sutton, U.K.). A549 (non-small cell lung cancer, human) and SW480 (colon carcinoma, human) cells were kindly provided by Brigitte Marian (Institute of Cancer Research, Department of Medicine I, Medical University of Vienna, Austria). Cells were grown in 75 cm^2 culture flasks (Iwaki/Asahi Technoglass) as adherent monolayer cultures in minimal essential medium (MEM) supplemented with 10% heat-inactivated fetal bovine serum, 1 mM sodium pyruvate and 2 mM L-glutamine (all purchased from Sigma-Aldrich) without antibiotics. Cultures were maintained at 37 °C in a humidified atmosphere containing 5% CO_2 and 95% air.

Table 1
Crystal data and details of data collection for **1**·H_2O.

	1·H_2O
Empirical formula	$C_{14}H_{15}Cl_5N_4OOs$
Fw	622.75
Space group	$Cmc2_1$
a [Å]	7.1253(4)
b [Å]	26.669(2)
c [Å]	9.8100(5)
V [Å^3]	1864.1(2)
Z	4
λ [Å]	0.71073
ρ_{calcd} [g cm^{-3}]	2.219
Crystal size [mm^3]	0.40 × 0.20 × 0.05
T [K]	100
μ [mm^{-1}]	7.568
R_1[a]	0.0428
wR_2[b]	0.1068
GOF[c]	1.094

[a] $R_1 = \Sigma||F_o| - |F_c||/\Sigma|F_o|$.
[b] $wR_2 = \{\Sigma[w(F_o^2 - F_c^2)^2]/\Sigma[w(F_o^2)^2]\}^{1/2}$.
[c] GOF = $\{\Sigma[w(F_o^2 - F_c^2)^2]/(n-p)\}^{1/2}$, where n is the number of reflections and p is the total number of parameters refined.

2.6. Cytotoxicity in cancer cell lines

Cytotoxicity in the cell lines mentioned above was determined by the colorimetric MTT assay (MTT = 3-(4,5-dimethyl-2-thiazolyl)-2,5-diphenyl-2*H*-tetrazolium bromide, purchased from Fluka). For this purpose, cells were harvested from culture flasks by trypsinization and seeded in 100 µl/well aliquots in MEM supplemented with 10% heat-inactivated fetal bovine serum, 1 mM sodium pyruvate, 4 mM L-glutamine and 1% non-essential amino acids (100×) into 96-well microculture plates (Iwaki/Asahi Technoglass) in the following densities, to ensure exponential growth of untreated controls throughout the experiment: 1.5×10^3 (CH1), 4.0×10^3 (A549) and 2.5×10^3 (SW480) viable cells per well. Cells were allowed to settle and resume proliferation for 24 h and were then exposed to the test compounds by addition of 100 µl/well aliquots of appropriate dilutions in the same medium. After exposure for 96 h, medium was replaced by 100 µl/well RPMI 1640 medium (supplemented with 10% heat-inactivated fetal bovine serum and 4 mM L-glutamine) plus 20 µl/well solution of MTT in phosphate-buffered saline (5 mg/ml) (all purchased from Sigma-Aldrich). After incubation for 4 h, medium/MTT mixtures were removed, and the formazan formed by viable cells was dissolved in DMSO (150 µl/well). Optical densities at 550 nm (corrected for unspecific absorbance at 690 nm) were measured with a microplate reader (Tecan Spectra Classic) to yield relative quantities of viable cells as percentages of untreated controls, and 50% inhibitory concentrations (IC_{50}) were calculated by interpolation. Evaluation is based on at least two independent experiments, each comprising triplicate samples.

2.7. Animals

Six- to eight-week-old female CB-17 scid/scid (SCID) mice were purchased from Harlan Laboratories (San Pietro al Natisone, Italy). The animals were kept in a pathogen-free environment and every procedure was done in a laminar airflow cabinet. Experiments were carried out according to the Austrian and FELASA guidelines for animal care and protection.

2.8. Xenograft experiments

Hep3B cells (10^6) were injected (RPMI with 10% matrigel) subcutaneously into the right flank. Therapy was started when tumor nodules reached a mean size of 25 mm^3. Animals were treated with **1** and **2** (20 mg/kg dissolved in 0.9% NaCl before administration five times a week for two weeks). Animals were controlled for distress development every day and tumor size was assessed regularly by caliper measurement. Tumor volume was calculated using the formula: (length × width^2)/2. The drug effect was assessed by determining the tumor volume on day 25 and day 40.

3. Results and discussion

3.1. Synthesis

In our previous work [39] we described the synthesis of (azole) pentachloridoosmium(IV) complexes by exploring the Anderson rearrangement reaction (Hazole = azole heterocycle):

$$(H_2azole)_2\left[Os^{IV}Cl_6\right] \xrightarrow[-HCl]{} (H_2azole)\left[Os^{IV}Cl_5(Hazole)\right] \xrightarrow[-HCl]{} \left[Os^{IV}Cl_4(Hazole)_2\right].$$

Performing these transformations with imidazole and pyrazole in alcohols (85–130 °C) led to the formation of disubstituted products. Therefore, to quench the Anderson rearrangement after the first step, we carried out the reaction in the presence of tetrabutylammonium chloride. We succeeded to obtain $(n\text{-Bu}_4\text{N})[\text{Os}^{\text{IV}}\text{Cl}_5(\text{Hazole})]$ salts in boiling ethanol for 1*H*-pyrazole, 1*H*-indazole, 1*H*-benzimidazole, 1*H*,2,4-triazole in 24, 70, 79, and 33% yield, correspondingly. Imidazole analog was synthesized in isoamyl alcohol at 100 °C in minor yield, whereas in boiling ethanol $\{(n\text{-Bu}_4\text{N})_2[\text{Os}^{\text{IV}}\text{Cl}_6]\}_2\cdot[\text{Os}^{\text{IV}}\text{Cl}_4(\text{Him})_2]$ (Him = 1*H*-imidazole)was formed. The synthesis of $(n\text{-Bu}_4\text{N})[\text{Os}^{\text{IV}}\text{Cl}_5(\text{Hbzim})]$ (Hbzim = 1*H*-benzimidazole) was accompanied by concurrent formation of *trans*-$[\text{Os}^{\text{IV}}\text{Cl}_4(\text{Hbzim})_2]$.

The coordination mode of indazole in $(n\text{-Bu}_4\text{N})[\text{Os}^{\text{IV}}\text{Cl}_5(\text{Hind})]$, its sodium and indazolium salts was established by X-ray diffraction and NMR spectroscopy. This finding was in accord with a number of well-documented crystallographic studies, in which coordination of indazole to the metal ion takes place via the N2 nitrogen (in nomenclature terms used for 1*H*-indazole). Surprisingly, we have discovered now that the Anderson rearrangement reaction of $(\text{H}_2\text{ind})_2[\text{Os}^{\text{IV}}\text{Cl}_6]$ results in the formation of two isomers, $(\text{H}_2\text{ind})[\text{Os}^{\text{IV}}\text{Cl}_5(2H\text{-ind})]$ (**1**) and $(\text{H}_2\text{ind})[\text{Os}^{\text{IV}}\text{Cl}_5(1H\text{-ind})]$ (**2**) (Chart 2). The 2*H*-form of indazole in **1** is bound to osmium(IV) via nitrogen atom N1 (vide infra). To the best of our knowledge this is a second case of stabilization of 2*H*-form of indazole and its coordination to metal ions via N1 documented in the literature [40]. The synthesis and separation of the two isomers are straightforward and can be performed in a single step avoiding unnecessary intermediate transformations making these complexes available for comparative biological investigations.

3.2. Crystal structure

The crystal structure of $\mathbf{1}\cdot\text{H}_2\text{O}$ contains an essentially octahedral complex $[\text{Os}^{\text{IV}}\text{Cl}_5(2H\text{-ind})]^-$ (Fig. 1). The complex crystallized in the orthorhombic space group $Cmc2_1$. The asymmetric unit consists of half an anion, half a cation (disordered over two positions) and half a water molecule which are related with the corresponding second half by a plane of symmetry. It should be noted that the coordinated indazole is out of the symmetry plane and is therefore disordered over two positions as shown in Fig. 1. The indazolium cation is disordered over four (pairwise) symmetry related positions. The observed disorder in the crystal structure of $\mathbf{1}\cdot\text{H}_2\text{O}$ makes a close comparison of geometrical parameters of $[\text{Os}^{\text{IV}}\text{Cl}_5(2H\text{-ind})]^-$ and $[\text{Os}^{\text{IV}}\text{Cl}_5(1H\text{-ind})]^-$ irrelevant. Therefore only a few parameters are quoted in Table 2.

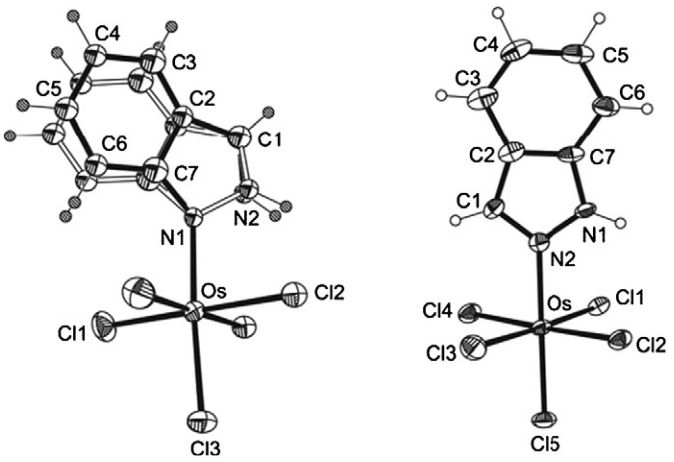

Fig. 1. The structure of the complex anions in **1** (left) and in $(n\text{-Bu}_4\text{N})[\text{Os}^{\text{IV}}\text{Cl}_5(1H\text{-ind})]$ (right). The coordinated 2*H*-indazole is disordered over two positions related by a plane of symmetry through Os1, three chlorido ligands, atoms N1 and C1.

The Os – Cl bonds in **1** and in $(n\text{-Bu}_4\text{N})[\text{Os}^{\text{IV}}\text{Cl}_5(1H\text{-ind})]$ [39] are commonly significantly longer than in $(\text{Ph}_4\text{P})[\text{Os}^{\text{V}}\text{Cl}_6]$ [48] at 2.252(4)–2.295(2) or $(\text{Et}_4\text{N})[\text{Os}^{\text{V}}\text{Cl}_6]$ [49] at 2.295(3)–2.308(2) Å and well comparable to those in $(\text{HPPh}_3)_2[\text{Os}^{\text{IV}}\text{Cl}_6]\cdot\text{DMF}$ [50] at 2.330(5)–2.340(5) Å.

Indazole acts mainly as a monodentate neutral ligand in metal complexes binding to metal ions via N2. In a few cases, it was found to be deprotonated, acting as a bridging ligand in polynuclear metal complexes [51,52] or even more rarely as a monodentate indazolate ligand coordinated via N1 or N2 [53,54].

3.3. EPR measurements

Compound **1** was investigated by X-band EPR spectroscopy at 77 K in 1:1 v/v DMF/MeOH solution (8 mM). A very weak, nearly axial EPR signal was observed (Supporting Information, Fig. S1) with g = 2.64(1), 2.53(1), 2.03(5), which resembles signals seen for ruthenium(III) analogs [55], as well as for other low-spin d^5 complexes [56,57]. We attribute this signal to residual osmium(III) side material. EPR studies of authentic osmium(III) complexes are in progress. No signals due to osmium(IV) or any other paramagnetic species (e.g., organic radicals) were observed. A detailed investigation of the magnetic and electronic properties of the Os(IV) complexes described herein is in progress and will be reported separately, as it is beyond the scope of the present study.

3.4. NMR spectra

It should be also stressed that both compounds remain intact in dimethylsulfoxide and the coordination mode can easily be established by NMR spectroscopy. The ^{1}H and ^{13}C NMR spectra show signals due to the H_2ind^+ cation and the coordinated indazole heterocycle. The integration is equal for each detected proton signal of both the coordinated indazole ligand and the indazolium cation.

The ^{1}H NMR spectrum of the H_2ind^+ cation is well resolved and shows, as expected, a singlet at 8.07 ($\text{H}_{3'}$), two doublets at 7.76 ($\text{H}_{4'}$) and 7.54 ($\text{H}_{7'}$) and two triplets at 7.11 ($\text{H}_{5'}$) and 7.34 ($\text{H}_{6'}$) ppm.

The signals of the coordinated indazole are markedly upfield shifted to negative values, especially for the protons which are closer to the (low-spin d^4) osmium(IV) metal center, which presumably possesses marked temperature-independent paramagnetism. However, it should be noted that the signals appear almost as sharp as in diamagnetic compounds. The multiplicity of ligand ^{1}H signals is the same as for the metal-free indazole but the order in which they appear changes due to coordination to the osmium atom.

From the ^{15}N,^{1}H HSQC plot of **1** the H_2 is seen at 14.25 ppm (Supporting Information, Fig. S2). A poorly resolved signal of C_3 was detected in ^{13}C,^{1}H HSQC plot at 299.7 ppm, whereas its proton (H_3) at −14.54 ppm. The cross-peak of C_3 with H_4 permits to assign two doublets (H_4 is at 2.81 and H_7 at 4.52 ppm). Protons H_4 and H_7 show a coupling in ^{1}H, ^{1}H COSY plot with H_5 (6.66 ppm) and H_6 (−0.43 ppm), correspondingly (Supporting Information, Fig. S3). Therefore four *C*H resonances of benzene ring are at 99.06 (C_7), 104.60 (C_5), 157.09 (C_4), and 177.15 (C_6) ppm. The quaternary carbon at 184.29 ppm (C_8) displays cross-peaks with H_4 and H_6, whereas the signal at 58.55 ppm (C_9) couples with H_5 and H_7 as can be seen in the ^{13}C,^{1}H HMBC plot (Supporting Information, Fig. S4).

The ^{1}H NMR spectra of the coordinated to osmium(IV) 1*H*-indazole and its 2*H*-tautomer differ significantly. In particular the chemical shift

Table 2
Selected bond distances (Å) in $(\text{H}_2\text{ind})[\text{Os}^{\text{IV}}\text{Cl}_5(2H\text{-ind})]$ (**1**) and in $(n\text{-Bu}_4\text{N})[\text{Os}^{\text{IV}}\text{Cl}_5(1H\text{-ind})]$ [39].

Atom1–atom2	**1**	$(n\text{-Bu}_4\text{N})[\text{Os}^{\text{IV}}\text{Cl}_5(1H\text{-ind})]$
Os–N1/Os–N2	2.067(13)	2.068(3)
$\text{Os–Cl}_{\text{axial}}$	2.353(4)	2.3332(10)
$\text{Os–Cl}_{\text{equatorial}}$(av)	2.328(13)	2.325(11)

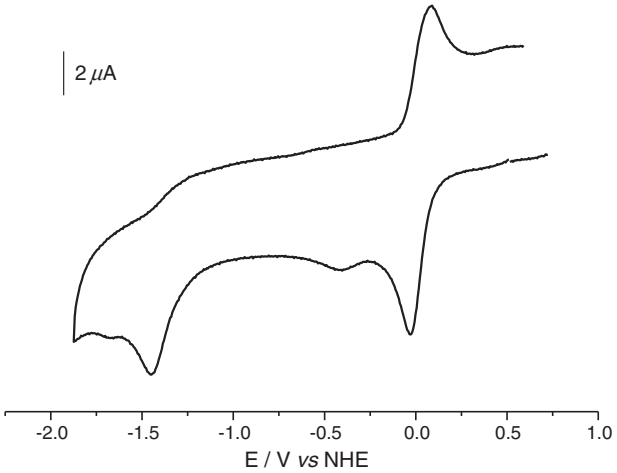

Fig. 2. Cyclic voltammogram of 0.2 M **1** in DMSO at a carbon disk working electrode and a scan rate of 0.2 V/s, starting the scan in cathodic direction.

of H_3 differs for **1** and **2** by ca. 10 ppm. In addition, the position of *N*H signal differs by 38.8 ppm (δ 124.7 ppm for $[Os^{IV}Cl_5(1H\text{-ind})]^-$ and 85.9 ppm for $[Os^{IV}Cl_5(2H\text{-ind})]^-$). A significant downfield shift of C_3 resonance in **1** by 99.04 ppm compared to that in $[Os^{IV}Cl_5(1H\text{-ind})]^-$ at 200.66 ppm is also of note. The shifts of other carbon signals are in the range from 1.55 to 17.51 ppm (in $[Os^{IV}Cl_5(1H\text{-ind})]^-$ the carbon resonances are at 75.94 (C_9), 81.88 (C_7), 106.16 (C_5), 139.58 (C_4), 163.74 (C_6) and 173.67 (C_8) ppm) [39].

3.5. Electrochemical behavior

The cyclic voltammograms (CV) of **1** and **2** in DMSO (0.2 M (n-Bu_4N)[BF_4]/DMSO) at a carbon disk working electrode, recorded with a scan rate of 0.2 V/s, display a reversible one-electron reduction wave attributed to the $Os^{IV} \rightarrow Os^{III}$ process with a potential value of 0.03 and 0.13 V for **1** and **2** respectively. Irreversible single electron reduction wave (I^{red}) attributed to the $Os^{III} \rightarrow Os^{II}$ process is observed at −1.43 (Fig. 2) and −1.33 V for **1** and **2**, correspondingly. The redox waves Os^{IV}/Os^{III} for **1** and **2** are characterized by a peak-to-peak separation (ΔE_p) of 74 and 95 mV respectively, and an anodic peak current (i_{pa}) that is almost equal to the cathodic peak current (i_{pc}) in both cases, as expected for a reversible electron transfer process. The one-electron nature of the electron transfer process was verified by comparing the peak current height (i_p) with that of the standard ferrocene/ferrocenium couple under the same experimental conditions. The application of Lever's equation [58] (Eq. (1)) [E_L(Cl) = −0.24 [59], $S_M(Os^{III}/Os^{II}) = 1.01$ [59], and $I_M(Os^{III}/Os^{II}) = -0.40$ [59]]

$$E = S_M \sum E_L + I_M \quad (1)$$

for $Os^{III} \rightarrow Os^{II}$ process has allowed the estimate of the yet unknown E_L ligand parameter for 2*H*-ind tautomer (**1**, $E_L = 0.18$ V), whereas E_L ligand parameter for 1*H*-ind tautomer in **2**, according to Eq. (1), is 0.28 V. Reported E_L value for 1*H*-ind tautomer is 0.26 V [20].

This finding demonstrates the increase of the net electron-donor character (decrease of E_L) of 2*H*-ind tautomer compared to 1*H*-ind tautomer, which results in decreased reduction potential of **1**.

3.6. UV–vis spectra, aqueous solubility and resistance to hydrolysis

The aqueous solubility of **1** is 1.2 mM at 298 K, compared to 1.3 mM for **2**. The aqueous solution behavior of **1** and **2** with respect to hydrolysis was studied by optical spectroscopy at 294 K over 24 h (Fig. 3). Both complexes are stable in aqueous solution. Immediate hydrolysis was excluded since the peak at m/z 485 assigned to $[Os^{IV}Cl_5(Hind)]^-$ was observed in the negative ion ESI mass spectrum of the aqueous solution of both **1** and **2** after 24 h. The UV–vis spectra of **1** and **2** are compared in Fig. 4.

3.7. Solvatochromism

Solvatochromic studies on complexes **1** and **2** have been carried out by using water and a number of common organic solvents. Complex **1** shows red shifts of the absorption maxima (510–560 nm) in the following order: DMF > THF > DMSO > H_2O (Fig. 5), which is not strictly in line with the relative permittivity values (ε_r) of tetrahydrofurane (7.5) [60], dimethylformamide (37.31) [61], dimethylsulfoxide (47.2) [62], and water (80.2) [63]. The shift on going from one organic solvent to another is small relatively to that observed on going from dimethyl sulfoxide to water. A dramatic increase of the extinction coefficient of the mostly long-wavelength absorption in aqueous solution is also of note. The solvatochromic behavior of **2** is similar. A red shift on going from organic solvents to water is also clearly seen, although the extinction coefficients for the red shifted bands are much lower than for those in **1** (see Supporting Information, Figs. S5 and S6). The solvatochromic behavior of compounds is usually explained through different solvation of the ground and excited states, the positive solvatochromism resulting from better stabilization of the excited state by polar solvents. However, this traditional approach, in which only the equilibrium solvation of the ground and excited states is taken into account sometimes fails [64–66].

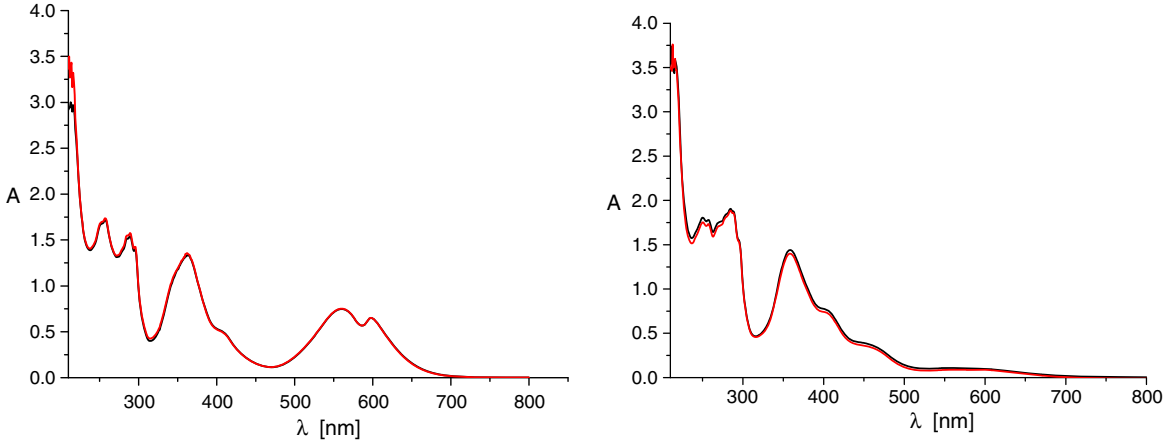

Fig. 3. UV–vis spectra of an aqueous solution of **1** (left) and **2** (right), measured immediately after dissolution and 24 h thereafter.

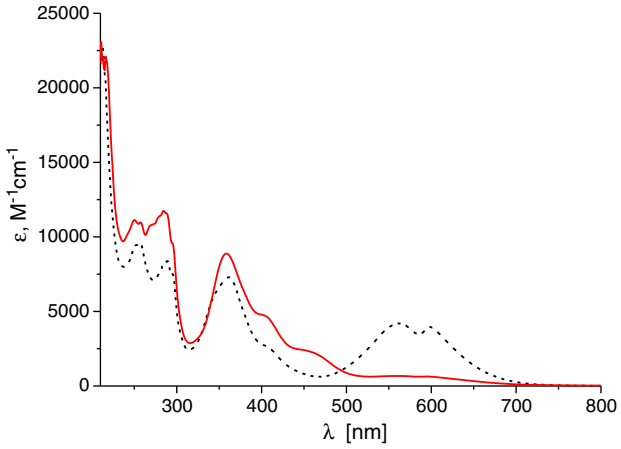

Fig. 4. UV–vis spectra of aqueous solutions of **1** (dashed black line) and **2** (solid red line).

Therefore, the conclusion about the polarity of the ground and excited states on the basis of solvatochromic studies is no longer obvious [67]. In the present case the strong red shift of the visible bands in water solution should be ascribed to a large electric dipole moment in the excited state in this spectroscopic domain. This implies a large contribution of charge transfer bands in the visible region, which could be tentatively assigned as involving the electron transfer from indazole to osmium. Indeed, as can be envisaged from Fig. 1, a variation of the dipole moment of the order of several Debye could be expected for such an electron transfer. The nature of the excited states in the visible region is currently investigated by ab initio calculations.

3.8. Stability and mutual transformation of isomers

The isomeric complexes **1** and **2** were stable in aqueous solution for at least 24 h (see Section 3.6.) and in dimethyl sulfoxide for at least 96 h at room temperature. Attempts to induce tautomer conversion by UV irradiation (in ethanolic solution, 150 W Heraeus Noblelight) resulted in disappearance of the ^{1}H NMR resonances of the coordinated azole heterocycle after 15 min and in disappearance of the free indazole signals and formation of ammonium ion after 1 h of irradiation. Heating **1** and **2** under the conditions used for their synthesis (see Section 2.2.) for 6 h led to their minor conversion (less than 10%) into **2** and **1**, respectively, according to integration of the proton resonances. In addition, formation of trace amounts of $[OsCl_4(Hind)_2]$ has been detected in solution by NMR spectroscopy. These data along with the isolation of both isomers from the same synthesis with comparable yields offer compelling evidence for close thermodynamic stability and reactivity of both isomers.

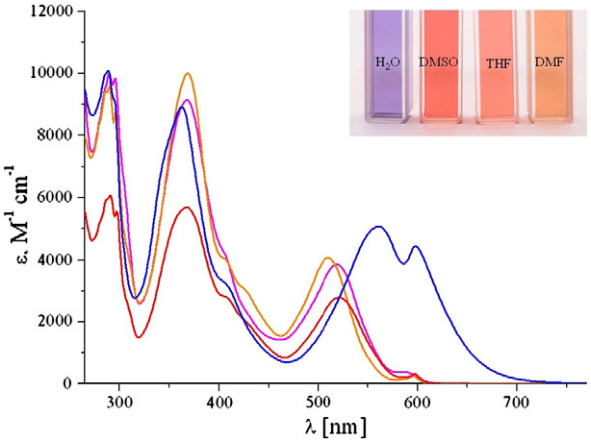

Fig. 5. UV–vis spectra of solutions of **1** in H_2O (blue), DMSO (red), THF (pink) and DMF (orange).

3.9. Cytotoxicity in cancer cell lines

The cytotoxicity of **1**, in which the ligand adopts the 2*H*-indazole tautomeric form, was compared to that of the analogous 1*H*-indazole complex **2** by means of the MTT assay in three human cell lines originating from different malignant tumors. A 96 h exposure yielded the concentration–effect curves depicted in Fig. 6.

Whereas the curves closely resemble each other in the ovarian carcinoma cell line CH1 (IC_{50}: 92 ± 20 μM vs 98 ± 23 μM for **1** and **2**, respectively) and the colon carcinoma cell line SW480 (IC_{50}: 100 ± 15 vs 110 ± 6 μM), those in the non-small cell lung cancer cell line A549 show differences clearly exceeding the ranges of individual

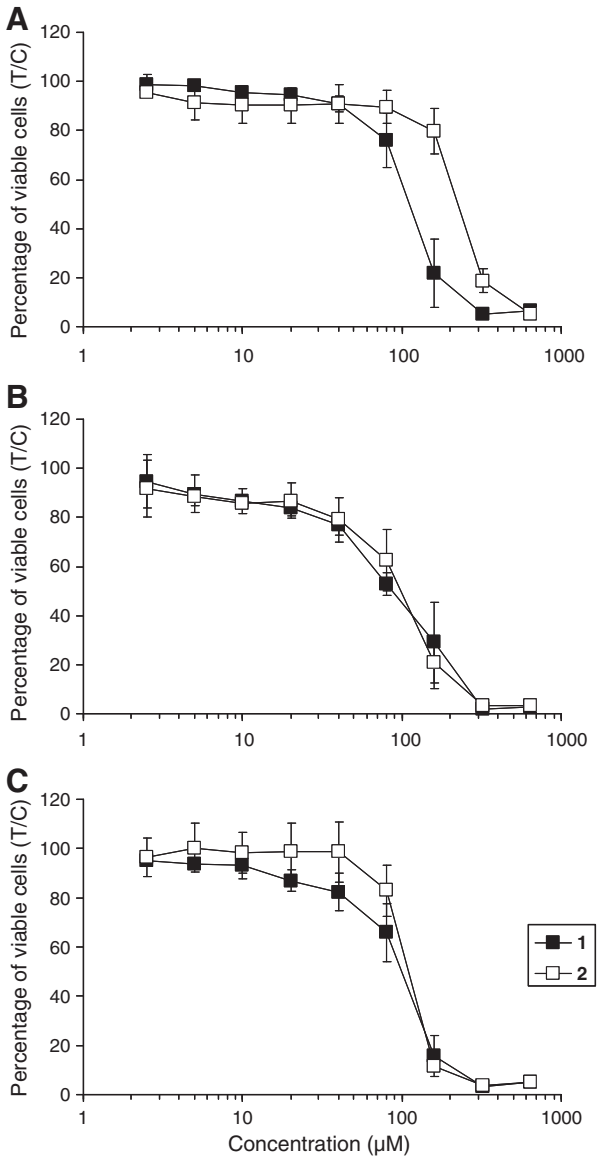

Fig. 6. Concentration–effect curves of $(H_2ind)[Os^{IV}Cl_5(2H\text{-ind})]$ (**1**) and $(H_2ind)[Os^{IV}Cl_5(1H\text{-ind})]$ (**2**) in (A) A549, (B) CH1 and (C) SW480 cells, obtained by the MTT assay (96 h exposure). Values are means ± standard deviations from at least two independent experiments.

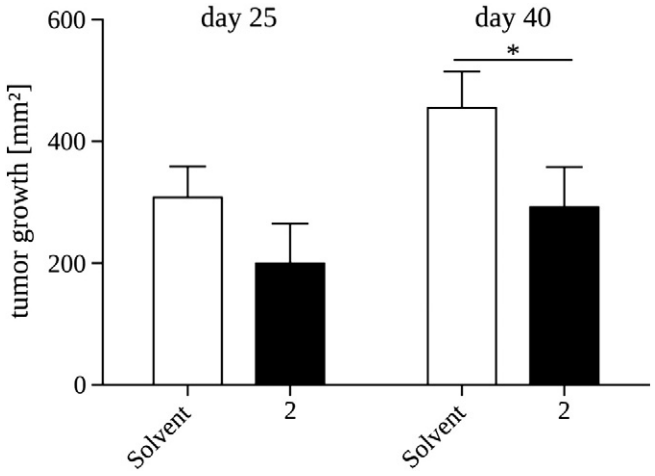

Fig. 7. Anticancer activity of the **2** in vivo. Hep3B xenografts were grown in Balb/c SCID mice and treated with **2** (20 mg/kg; i.v.; five consecutive days per week for 2 weeks). The effect of treatment on tumor growth on days 25 and 40 are shown: *$p<0.05$ (student's *t* test, Graph Pad Prism Software).

variations, with **1** being about twice as potent as **2** according to IC_{50} values (113 ± 17 vs 224 ± 18 μM). Thus, the generally more chemoresistant A549 cells are virtually as sensitive to **1** as the other two cell lines.

Taking into account the aqueous stability of the investigated compounds compared to rapid hydrolysis of ruthenium complexes, the mechanism of osmium complex cytotoxicity remains an open question.

3.10. Antiproliferative activity in vivo

Based on our *in vitro* results, we used a Hep3B SCID mouse xenotransplantation model to test the anticancer activity of **1** and **2** *in vivo*. In general, the drugs were well tolerated and the mice did not exhibit any symptoms of toxicity, such as fatigue, or significant weight loss. With regard to the anticancer activity, **2** induced a minor but significant delay in tumor growth (Fig. 7). The mean tumor volumes were decreased from 300 mm^2 to 200 mm^2 on day 25 and from 460 mm^2 to 290 mm^2 on day 40, respectively. In contrast, treatment with **1** did not result in lowered tumor mass (data not shown). Interestingly, however, this compound reduced the incidence of tumor necrosis. While control animals frequently had to be sacrificed due to bleeding of relatively small lesions, tumors in **1**-treated animals exhibited more benign growth leading to enhanced survival in a subgroup of animals (data not shown).

4. Final remarks

The Anderson type rearrangement of $(H_2ind)_2[Os^{IV}Cl_6]$ in ethanolic solution yielded two different products, $(H_2ind)[Os^{IV}Cl_5(2H\text{-ind})]$ and $(H_2ind)[Os^{IV}Cl_5(1H\text{-ind})]$. The established coordination mode of 2*H*-indazole via the N1 nitrogen atom in **1** has only one precedence in the coordination chemistry of indazole. Complexes **1** and **2** exhibit similar solvatochromic behavior. The cytotoxicity data suggest that complexes containing 2*H*-indazole might be advantageous over 1*H*-indazole-containing analogs with regard to inhibition of tumor cell growth in particular cell lines. In contrast to this the *in vivo* model showed only tumor growth inhibition for **2** but an interesting reduction of tumor necrosis and enhanced survival for mice treated with **1**. Efforts by us will be now focused on the synthesis of complexes of 2*H*-indazoles and evaluation of their cytotoxicity in order to obtain antitumor drugs, which are more effective than KP1019.

Acknowledgment

We thank Prof. Joshua Telser (Roosevelt University) for the EPR measurements and helpful comments, Prof. Liviu Chibotaru (Leuven University) for valuable comments, Alexander Roller for collecting the X-ray diffraction data and Prof. Dr. Markus Galanski for recording 2D NMR spectra. We are also indebted to the Austrian Science Fund (FWF) for financial support of the project I 374-N19.

Appendix A. Supplementary data

Supporting Information Available: EPR measurement for **1** (Fig. S1), $^{15}N,^{1}H$ HSQC, $^{1}H,^{1}H$ COSY and $^{13}C,^{1}H$ HMBC plots of **1** (Figs. S2–S4); UV–vis spectra of **2** in THF, MeOH, DMSO, DMF and H_2O (Figs. S5, S6). Crystallographic data for the structure of **1** reported in this paper have been deposited with the Cambridge Crystallographic Data Center as supplementary publication no CCDC 865239. Copies of the data can be obtained free of charge on application to The Director, CCDC, 12 Union Road, Cambridge CB2 1EZ, UK (fax: +44-1223-336-033; e-mail: deposit@ccdc.cam.ac.uk).

Supplementary data to this article can be found online at doi:10.1016/j.jinorgbio.2012.04.001.

References

[1] A. Schmidt, A. Beutler, B. Snovydovych, Eur. J. Org. Chem. (2008) 4073–4095.
[2] A. Rahman, S. Malik, H. Cun-heng, J. Clardy, Tetrahedron Lett. 26 (1985) 2759–2762.
[3] Y.-M. Liu, J.-S. Yang, Q.-H. Liu, Chem. Pharm. Bull. 52 (2004) 454–455.
[4] A. Rahman, S. Malik, S.S. Hasan, M.I. Choudhary, C.-Z. Ni, J. Clardy, Tetrahedron Lett. 36 (1995) 1993–1996.
[5] E.L. Elliott, S.M. Bushell, M. Cavero, B. Tolan, T.R. Kelly, Org. Lett. 7 (2005) 2449–2451.
[6] K. Inamoto, M. Katsuno, T. Yoshino, Y. Arai, K. Hiroya, T. Sakamoto, Tetrahedron 63 (2007) 2695–2711.
[7] W. Stadlbauer, Sci. Synth. 12 (2002) 227–235.
[8] H. Cerecetto, A. Gerpe, M. González, V.J. Arán, C.O. de Ocáriz, Mini Rev. Med. Chem. 5 (2005) 869–878.
[9] S. Huang, R. Li, P.J. Connolly, S. Emanuel, A. Fuentes-Pescuera, M. Adams, R.H. Gruninger, J. Seraj, S.A. Middleton, J.M. Davis, D.F.C. Moffat, Bioorg. Med. Chem. Lett. 17 (2007) 2179–2183.
[10] L. Bouissane, S. El-Kazzoulli, S. Léonce, B. Pfeiffer, E.M. Rakib, M. Khouili, G. Guillaumet, Bioorg. Med. Chem. 14 (2006) 1078–1088.
[11] P.J. Hesketh, D.R.J. Gandara, Nat. Cancer Inst. 83 (1991) 613–620.
[12] S.-L. Pan, J.-H. Guh, C.-Y. Peng, S.-W. Wang, Y.-L. Chang, F.-C. Cheng, J.-H. Chang, S.-C. Kuo, F.-Y. Lee, C.-M. Teng, J. Pharmacol. Exp. Ther. 314 (2005) 35–42.
[13] G. Daidone, D. Raffa, B. Maggio, M.V. Raimondi, F. Plescia, D. Schillaci, Eur. J. Med. Chem. 39 (2004) 219–224.
[14] D. Simoni, R. Romagnoli, R. Baruchello, R. Rondanin, M. Rizzi, M.G. Pavani, D. Alloatti, G. Gianinni, M. Marcellini, T. Riccioni, M. Castorina, M.B. Guglielmi, F. Bucci, P. Carminati, J. Med. Chem. 49 (2006) 3143–3152.
[15] G.A. Pinna, M.A. Pirisi, J.-M. Mussinu, G. Murineddu, G. Loriga, A. Pau, G.E. Grella, Farmaco 58 (2003) 749–763.
[16] A.P. Krapcho, S.N. Haydar, J. Heterocycl. Chem. 38 (2001) 1153–1166.
[17] M. Galanski, V.B. Arion, M.A. Jakupec, B.K. Keppler, Curr. Pharm. Des. 9 (2003) 2078–2089.
[18] M.A. Jakupec, M. Galanski, V.B. Arion, C.G. Hartinger, B.K. Keppler, Dalton Trans. (2008) 183–194.
[19] E. Alessio, G. Mestroni, B. Bergamo, G. Sava, Curr. Top. Med. Chem. 4 (2004) 1525–1535.
[20] E. Reisner, V.B. Arion, M.F.C. Guedes da Silva, R. Lichtenecker, A. Eichinger, B.K. Keppler, V.Yu. Kukushkin, A.J.L. Pombeiro, Inorg. Chem. 43 (2004) 7083–7093.
[21] B. Cebrián-Losantos, A.A. Krokhin, I.N. Stepanenko, R. Eichinger, M.A. Jakupec, V.B. Arion, B.K. Keppler, Inorg. Chem. 46 (2007) 5023–5033.
[22] F. Benetollo, A. Del Pra, L. Baiocchi, Farmaco 45 (1990) 1361–1367.
[23] F. Benetollo, A. Del Pra, F. Orsini, L. Baiocchi, J. Crystallogr. Spectrosc. Res. 23 (1993) 987–992.
[24] A. Escande, J. Lapasset, Acta Crystallogr. B30 (1974) 2009–2012.
[25] I. Leban, B. Stanovnik, M. Tisler, Acta Crystallogr. B34 (1978) 293–295.
[26] R.C. Gearhart, R.H. Wood, P.C. Thorstenson, J.A. Moore, J. Org. Chem. 39 (1974) 1007–1008.
[27] R. Krishnan, S.A. Lang, Y.I. Lin, R.G. Wilkinson, J. Heterocycl. Chem. 25 (1988) 447–452.
[28] S. Nan'ya, K. Katsuraya, E. Maekawa, K. Kondo, S. Eguchi, J. Heterocycl. Chem. 24 (1987) 971–975.
[29] A.J. Boulton, N. Henderson, A.K. Powell, B.R.F. Bracke, A.T.H. Lenstra, L.J. Vanmaele, J. Org. Chem. 56 (1991) 5278–5281.
[30] D.S. Coombes, S.L. Price, D.J. Willock, M. Leslie, J. Phys. Chem. 100 (1996) 7352–7360.

[31] K.W.F. Kohlrausch, R. Seka, Ber. Dtsch. Chem. Ges. 73 (1940) 162–166.
[32] J. Elguero, A. Fruchier, R. Jacquier, Bull. Soc. Chim. Fr. (1966) 2075–2084.
[33] F. Tröndlin, R. Werner, C. Rüchardt, Chem. Ber. (111) (1978) 367–378.
[34] J. Elguero, Pyrazoles and their benzo derivatives, Comprehensive Heterocyclic Chemistry, Pergamon Press, Oxford, 1984, pp. 291–297.
[35] J.W. Longworth, R.O. Rahn, R.G. Shulman, J. Chem. Phys. 45 (1966) 2930–2939.
[36] Z. Kazimerczuk, H. Lönnberg, J. Vilpo, W. Pfleiderer, Nucleosides Nucleotides 8 (1989) 599–617.
[37] F. Seela, W. Bourgeois, Helv. Chim. Acta 74 (1991) 315–322.
[38] L. Mosti, G. Menozzi, P. Fossa, P. Schenone, E. Lampa, C. Parrillo, M. D'Amico, F. Rossi, Farmaco 47 (1992) 567–584.
[39] G.E. Büchel, I.N. Stepanenko, M. Hejl, M.A. Jakupec, V.A. Arion, B.K. Keppler, Inorg. Chem. 48 (2009) 10737–10747.
[40] G.E. Büchel, I.N. Stepanenko, M. Hejl, M.A. Jakupec, B.K. Keppler, V.B. Arion, Inorg. Chem. 50 (2011) 7690–7697.
[41] G. Brauer, Handbuch der Präparativen Anorganischen Chemie, III, 1981, pp. 1742–1744.
[42] O.V. Rudnitskaya, T.M. Buslaeva, N.N. Lyalina, Zh. Neorg. Khim. 39 (1994) 922–924.
[43] I.N. Stepanenko, A.A. Krokhin, R.O. John, A. Roller, V.B. Arion, M.A. Jakupec, B.K. Keppler, Inorg. Chem. 47 (2008) 7338–7347.
[44] W.C. Barrette Jr., H.W. Johnson Jr., D.T. Sawyer, Anal. Chem. 56 (1984) 1890–1898.
[45] AINT-Plus, Version 7.06a and APEX2, Bruker-Nonius AXS Inc., Madison, WI, 2004.
[46] G.M. Sheldrick, Acta Crystallogr. A46 (2010) 112–122.
[47] G.K. Johnson, Report ORNL-5138, OAK Ridge National Laboratory, Oak Ridge, TN, 1976.
[48] E.E. Kim, K. Eriks, R. Magnuson, Inorg. Chem. 23 (1984) 393–397.
[49] B. Krebs, G. Henkel, M. Dartmann, W. Preetz, M. Bruns, Z. Naturforsch. 39b (1984) 843–849.
[50] P.D. Robinson, C.C. Hinckley, M. Matusz, P.A. Kibala, Acta Crystallogr. C44 (1988) 619–621.
[51] D.F. Rendle, A. Storr, J. Trotter, Can. J. Chem. 53 (1975) 2930–2943.
[52] S.A. Cortes-Llamas, J.M. Hernández-Pérez, M. Hó, M.-A. Munoz-Hernández, Organometallics 25 (2006) 588–595.
[53] J.P. Fackler Jr., R.J. Staples, R.G. Raptis, Z. Kristallogr. 212 (1997) 157–158.
[54] R. Schuecker, R.O. John, M.A. Jakupec, V.B. Arion, B.K. Keppler, Organometallics 27 (2008) 6587–6595.
[55] J. Telser, V.B. Arion, unpublished results.
[56] B.R. McGarvey, Coord. Chem. Rev. 170 (1998) 75–92.
[57] H. Rieger, Coord. Chem. Rev. 135/136 (1994) 203–286.
[58] A.B.P. Lever, E.S. Dodsworth, Inorganic Electronic Structure and Spectroscopy, Wiley, New York, USA, 1999, pp. 277–290.
[59] A.B.P. Lever, Inorg. Chem. 29 (1990) 1271–1285.
[60] P. Roy, A.K. Jana, D. Das, D.N. Nath, Chem. Phys. Lett. 474 (2009) 297–301.
[61] J. Barthel, R. Bucher, B. Wurm, J. Mol. Liq. 98–99 (2002) 51–69.
[62] S.E. McLain, A.K. Soper, A. Luzar, J. Chem. Phys. 124 (2006) 074502/1-74502/12.
[63] M. Mohsen-Nia, H. Amiri, B. Jazi, J. Solution Chem. 39 (2010) 701–708.
[64] D. Laage, W.H. Thompson, M. Blanchard-Desce, J.T. Hynes, J. Phys. Chem. A 107 (2003) 6032–6046.
[65] J. Kabatc, B. Jedrzejewsska, P. Orlinski, J. Paczkowski, Spectrochim. Acta, Part A 62 (2005) 115–125.
[66] A. Gaplovsky, J. Donovalova, P. Magdolen, S. Toma, P. Zahradnik, Spectrochim. Acta, Part A 58 (2002) 363–371.
[67] P. Hrobárik, I. Sigmundová, P. Zahradnik, P. Kasák, V.A. Arion, E. Franz, K. Clays, J. Phys. Chem. C 114 (2010) 22289–22302.